Narrowband multi-channel filters

Hongfei Jiao (焦宏飞)[1,2*], Xinbin Cheng (程鑫彬)[1], Tao Ding (丁 涛)[1], Ganghua Bao (鲍刚华)[1], Xiaodong Wang (王孝东)[1], Pengfei He (贺鹏飞)[2], and Yonggang Wu (吴永刚)[1]

[1]*Institute of Precision Optical Engineering, Department of Physics, Tongji University, Shanghai 200092, China*

[2]*School of Aerospace Engineering and Applied Mechanics, Tongji University, Shanghai 200092, China*

[*]*E-mail: hfjiao927@gmail.com*

Received November 20, 2009

We propose and demonstrate two types of narrowband multi-channel filters: transmittance-integrated narrow-bandpass filter arrays and reflectance narrowband multi-channel filters. We develop a combinatorial etching technique possessing 32 elements on a single substrate with which to fabricate these integrated narrow bandpass filters. Double-chamber integrated optical filter arrays are fabricated by use of this etching technique. Reflectance can be achieved by combining metal and dielectric materials. These narrowband multi-channel filters and narrow bandpass filter arrays show good filtering features and can be utilized in many optical applications.

OCIS codes: 310.0310, 230.0230, 220.0220.

doi: 10.3788/COL201008S1.0192.

Narrowband optical filters are becoming increasingly crucial for various applications[1,2] such as laser cavity reflectors, wavelength-division multiplexing, and multispectral devices. Common narrowband optical filters include Fabry-Pérot filters[3], fiber Bragg gratings[4], waveguide grating filters[5], Mach-Zehnder interferometers[6], and acousto-optic filters[7].

Here, we present two types of narrowband multi-channel filters. The first type is the transmittance narrowband multi-channel filter which integrates narrow-bandpass filters that contain 32 elements on a single substrate. The other type is the reflectance mode, which combines the metal and dielectric materials to fabricate a reflectance multi-channel filter.

The Fabry-Pérot filter has different transmission peak positions corresponding to the different thicknesses of spacer layers. Therefore, the position of the transmission peak can be adjusted and the channel can be chosen by changing the thickness of the spacer layer using certain techniques[8]. If a series of variant thickness of the spacer layers can be fabricated at different positions in the same substrate, the integration of a series of narrowband filters can be realized[9]. Thus, a two-chamber multi-channel narrowband filter designed to fabricate the filter by adjusting the thickness of two spacer layers is created.

The original filter is designed to be sub|$(1H1L)^4$1H 4.64L$(1H1L)^9$1H 4.64L$(1H1L)^4$1H|air with the design wavelength of 777.4 nm, which is the characteristic peak of lightning. The spacer layer of the two-chamber filter is 4.64L, where sub is the substrate of K9 glass, $n_S = 1.52$, $n_A = 1$. H (the high-index material, TiO_2) and L (the low-index material, SiO_2) are $\lambda_0/(4n_H)$ and $\lambda_0/(4n_L)$, respectively, and $n_H = 2.16$, $n_L = 1.46$. If the optical thickness of the spacer layer is equidistantly decreased, a series of uniformly spaced channel narrowband filters can be realized.

Unlike the traditional preparation of the one-chamber integrated filter, the two resonant cavities of this integrated filter have to be etched in the preparation process because of the two-chamber structure. The etched thickness must be strictly equal, otherwise, the peak height of the narrowband will fall off or even completely disappear. The technique process is composed of five steps: 1) depositing $(1H1L)^4$1H 4.64L; 2) etching the first resonant cavity by ion-beam; 3) continued depositing $(1H1L)^9$1H 4.64L on the etched sample in the same vacuum chamber under the same condition; 4) etching the second resonant cavity of the sample by ion-beam through the third step; 5) depositing the residual membranous layer $(1H1L)^4$1H on the second etched sample under the same conditions. The procedure diagram for the fabrication of the filter is shown in Fig. 1. The improved dual extremum method monitoring the deposition is adopted based on the equipment conditions.

The depositing equipment in the experiment is the optical multi-layer coating machine ZZSX-800, where the electron beam vapor deposition method assisted by ionic bombardment to fabricate the multi-layer is conducted. The ion-beam etching machine LKJ-1C is used with the dry etching method. The entrance angle of the ion-beam is normal. The depth of the 32 parallel etched notches is gradually increased, creating the width and length of 0.375 and 12 mm, respectively.

The transmittances of the 32 channels are shown in Fig. 2(a), and the position distribution of the peaks is shown in Fig. 2(b). Figure 2(a) shows that every channel is distinctly separated, hence the preparation scheme is feasible. Although the height and width of some transmission peaks are not ideal, and the wavelength space between the adjacent channels is not strictly identical, these

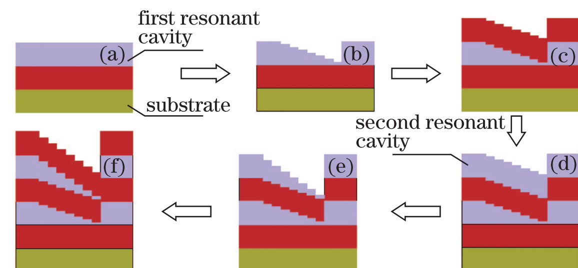

Fig. 1. Flow sheet of the preparation of the two-chamber integrated narrowband filter.

 © 2010 Chinese Optics Letters

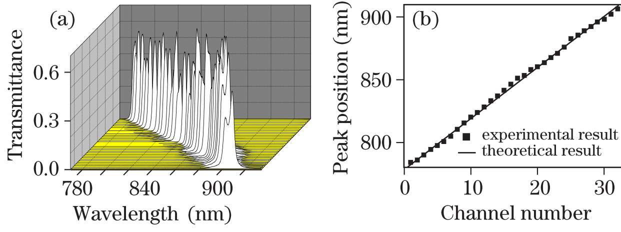

Fig. 2. (a) Transmittance curves of the 32 channels in the same substrate, and (b) the distribution of 32 channels.

correlate to the thickness controlling each layer and etched thickness of the first and second resonance cavities.

For decades, extensive studies on the design and fabrication of the transmittance filters have been carried out. Narrowband high-reflection filters have also found wide applications in optical communications and optical detectors, especially as their high-reflection compound multilayer filters consisting of metal and dielectric materials have more advantages in very narrow bands and sufficiently low sidebands. A novel method for constructing multi-channel narrowband high-reflection filters is proposed[10].

Firstly, the initial structure sub | $\mathrm{H(LH)}^{m_1}\mathrm{(LH)}^{m_2}$ $\mathrm{2L(HL)}^{m_2}$ is taken into consideration, where m_1 and m_2 are integers, and H and L are quarter-wave layers with high and low refractive indices, respectively. The calculated equivalent admittance for this structure at the central wavelength is expressed as

$$Y_1 = \frac{n_{\mathrm{H}}^2}{n_{\mathrm{S}}}\left(\frac{n_{\mathrm{H}}}{n_{\mathrm{L}}}\right)^{2m_1}, \tag{1}$$

where n_{S}, n_{H}, and n_{L} are the refractive indices of the substrate, and H and L layers, respectively. The equivalent admittance is real and becomes a large number when m_1 is sufficiently large. The reflectivity of a film stack can be described as

$$R = \left(\frac{\eta_0 - Y}{\eta_0 + Y}\right)\left(\frac{\eta_0 - Y}{\eta_0 + Y}\right)^* = \frac{(\eta_0 - Y_{\mathrm{r}})^2 + Y_{\mathrm{i}}^2}{(\eta_0 + Y_{\mathrm{r}})^2 + Y_{\mathrm{i}}^2}, \tag{2}$$

where η_0 stands for the admittance of the incident medium, $Y = Y_{\mathrm{r}} + \mathrm{i}Y_{\mathrm{i}}$ is the equivalent admittance of the stack, Y_{r} and Y_{i} are the real and imaginary part of Y, respectively. Equation 2 shows that the reflectivity of the structure is unity.

Subsequently, a thin metal layer M is attached to this structure to form the structure sub | $\mathrm{H(LH)}^{m_1}\mathrm{(LH)}^{m_2}$ $\mathrm{2L(HL)}^{m_2}\mathrm{M}$. If the refractive index n and the extinction coefficient k of the metal layer satisfy $n \approx k$, and the thickness d is far less than the radiation wavelength λ, the characteristic matrix of the metal layer can be expressed as

$$\begin{bmatrix} 1 & \mathrm{i}2\pi d/\lambda \\ 4\pi dnk/\lambda & 1 \end{bmatrix}.$$

The characteristic matrix for the composite structure becomes

$$\begin{bmatrix} B_2 \\ C_2 \end{bmatrix} = \begin{bmatrix} 1 & \dfrac{\mathrm{i}2\pi d}{\lambda} \\ \dfrac{4\pi dnk}{\lambda} & 1 \end{bmatrix} \begin{bmatrix} 1 \\ Y_1 \end{bmatrix} = \begin{bmatrix} 1 + \dfrac{\mathrm{i}Y_1 2\pi d}{\lambda} \\ \dfrac{4\pi dnk}{\lambda} + Y_1 \end{bmatrix}. \tag{3}$$

Accordingly, the equivalent admittance of the structure is represented by

$$Y_2 = \frac{C_2}{B_2} = \left(\frac{4\pi dnk}{\lambda} + Y_1\right) \Big/ \left(1 + \frac{\mathrm{i}Y_1 2\pi d}{\lambda}\right). \tag{4}$$

Because the value of Y_1 is large, the absolute value of the second term is much greater than the first term in the denominator. Therefore, Y_2 is imaginary. The reflectivity is unity, according to Eq. 2.

Finally, a dielectric match-stack $\mathrm{M_d}$ composed of several layers of materials with alternating high and low refractive indices is attached to sub | $\mathrm{H(LH)}^{m_1}$ $\mathrm{(LH)}^{m_2}\mathrm{2L(HL)}^{m_2}\mathrm{M}$ to form the structure sub | $\mathrm{H(LH)}^{m_1}$ $\mathrm{(LH)}^{m_2}\mathrm{2L(HL)}^{m_2}\mathrm{MM_d}$. The characteristic matrix of the match-stack is

$$\begin{bmatrix} m_{11} & \mathrm{i}m_{12} \\ \mathrm{i}m_{21} & m_{22} \end{bmatrix},$$

where m_{11}, m_{12}, m_{21}, and m_{22} are real. The characteristic matrix of the resulting structure becomes

$$\begin{bmatrix} B_3 \\ C_3 \end{bmatrix} = \begin{bmatrix} m_{11} & \mathrm{i}m_{12} \\ \mathrm{i}m_{21} & m_{22} \end{bmatrix} \begin{bmatrix} 1 \\ Y_2 \end{bmatrix} = \begin{bmatrix} m_{11} + \mathrm{i}m_{12}Y_2 \\ \mathrm{i}m_{21} + m_{22}Y_2 \end{bmatrix}. \tag{5}$$

Accordingly, the equivalent admittance of the structure is

$$Y_3 = \frac{C_3}{B_3} = \frac{\mathrm{i}m_{21} + m_{22}Y_2}{m_{11} + \mathrm{i}m_{12}Y_2}. \tag{6}$$

Because Y_2 is imaginary, the equivalent admittance Y_3 is also imaginary. Therefore, the reflectivity of the structure becomes unity, according to Eq. 2.

Based on the above analysis, reflectivity is always unity at the central wavelength regardless of the structure, whether it is sub | $\mathrm{H(LH)}^{m_1}\mathrm{(LH)}^{m_2}\mathrm{2L(HL)}^{m_2}$, sub | $\mathrm{H(LH)}^{m_1}\mathrm{(LH)}^{m_2}\mathrm{2L(HL)}^{m_2}\mathrm{M}$, or sub | $\mathrm{H(LH)}^{m_1}\mathrm{(LH)}^{m_2}$ $\mathrm{2L(HL)}^{m_2}\mathrm{MM_d}$. Therefore, a means to reduce reflection in the sidebands of the structure Sub | $\mathrm{H(LH)}^{m_1}$ $\mathrm{(LH)}^{m_2}\mathrm{2L(HL)}^{m_2}$ without impairing the high reflectivity at the central wavelength is by adding a thin metal layer with $n \approx k$ and a dielectric match-stack, and subsequently optimizing their thickness and configuration.

It is logical to generalize the above analysis to locate where either high-reflection peak occurs at non-central wavelength or multiple reflection peaks occur. If, at the non-central wavelength or at several arbitrary wavelengths, the real part of the equivalent admittance of the initial structure is a large number and the imaginary part is zero, the reflectivity will remain unity at those wavelengths after a thin metal layer with $n \approx k$ and a dielectric match-stack are added to the structure. Furthermore, the thickness of the metal layer and the configuration of the dielectric match-stack can be optimized to achieve low-reflection sidebands around the high-reflection peaks.

Figure 3 shows the real and imaginary parts of the equivalent admittance as a function of the wavelength of the incident EM wave of the structure sub | $\mathrm{H(LH)}^{13}\mathrm{(LH)}^2\mathrm{(2L2H)}^3\mathrm{2L(HL)}^2$, where the middle part is $\mathrm{(LH)}^2\mathrm{(2L2H)}^3\mathrm{2L(HL)}^2$. The real part of the admittance is a large number at the wavelength ratios (λ_0/λ) 0.9, 1.0, and 1.1 (Fig. 3(a)), while the imaginary part

is zero (Fig. 3(b)). Based on the aforementioned analysis, a metal layer satisfying the condition $n \approx k$ and a dielectric match-stack can be added to this structure, and their thickness and configuration can be optimized to obtain a multi-wavelength reflection filter. This also suggests that a multi-wavelength reflection filter with adjustable reflection peak positions may be realized by properly constructing the middle structure.

According to the principle of reflectance multi-channel filters, the peak positions can be adjusted by modifying the thickness of spacer layer. Taking structure sub | $H(LH)^{15}\alpha L$ $(HL)^5$ $Cr_{9.4}$ 0.49H 0.61L | air (Fig. 4) as an example, the position of the narrow reflection band could be readily adjusted by altering the thickness of the spacer layer αL.

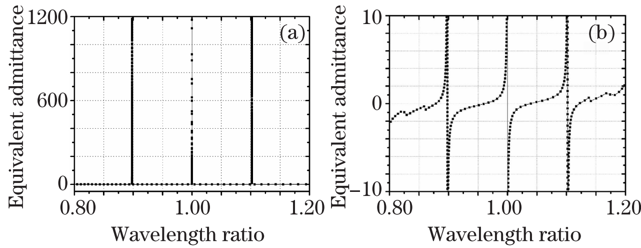

Fig. 3. Equivalent admittance versus wavelength ratio of the indent EM wave of the structure sub | $H(LH)^{13}(LH)^2$ $(2L2H)^3 2L(HL)2$ in (a) real part, and (b) imaginary part.

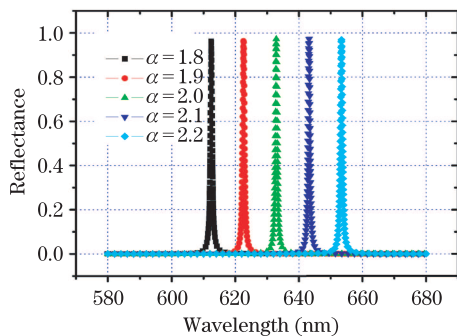

Fig. 4. Positions of the reflection band with regard to the thickness of the spacer layer for the structure sub| $H(LH)^{15}\alpha L(HL)^5 Cr_{9.4}0.49H0.61L$|air.

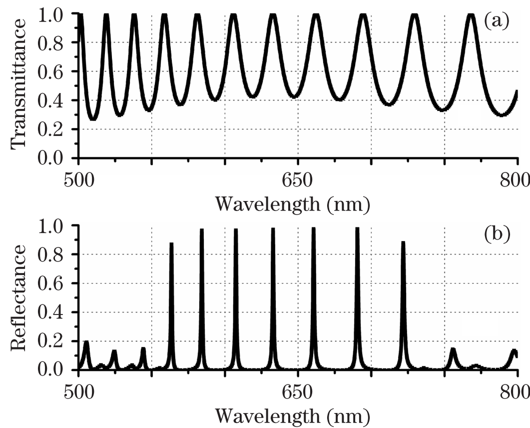

Fig. 5. Transmission spectrum of (a) $(LH)^2(2L2H)^{10}2L(HL)^2$ and the reflection spectrum of (b) sub | $H(LH)^{13}(LH)^2$ $(2L2H)^{10}2L(HL)^2Cr_{9.4}0.49H0.61L$.

This work also studies the effect of flanking the middle structure with stacks $(LH)^q$ and $(HL)^q$ or with sub | $H(LH)^{13}$ and $Cr_{9.4}0.49H0.61L$ on the transmission and reflection spectra, especially on the position of the transmission and reflection peaks.

The structures $(LH)^2(2L2H)^{10}2L(HL)^2$ and sub | $H(LH)^{13}(LH)^2(2L2H)^{10}2L(HL)^2Cr_{9.4}0.49H$ 0.61L are chosen as examples. The former can be treated as a middle structure and the latter is obtained by flanking the former with sub | $H(LH)^{13}$ and $Cr_{9.4}0.49H0.61L$. The calculated transmission spectrum of the former and the reflection of one of the latter are shown in Fig. 5(a) and (b), respectively. In the calculation, the condition $n_S = 1$, $n_H = 2.16$, $n_L = 1.46$, and $\lambda_0 = 632.8$ nm is adopted.

The number of peaks in both the transmission spectrum of the structure $(LH)^2(2L2H)^{10}2L(HL)^2$ and the reflection spectrum of the structure sub | $H(LH)^{13}$ $(LH)^2(2L2H)^{10}2L(HL)^2Cr_{9.4}0.49H0.61L$ is identical in the wavelength range of 550–750 nm. In addition, the peak positions are nearly identical. This indicates that the peak number and peak position of multi-wavelength reflection filters are determined, to a great extent, by the middle structure. Although the peak position of the transmission spectrum and that of the reflection spectrum are absolutely identical at the central wavelength, as shown in Figs. 5(a) and (b), a deviation of the reflection peaks from the transmission ones at the wavelengths other than the central one is observed. The further the peak is from the central wavelength, the larger the deviation becomes. This can be attributed to the relatively high reflectivity of the flanking film stacks sub | $H(LH)^{13}$ and $Cr_{9.4}0.49H0.61L$, which means high barriers exist in the structure sub | $H(LH)^{13}$ $(LH)^2(2L2H)^{10}2L(HL)^2Cr_{9.4}0.49H0.61L$.

To decipher the cause for the deviation, film stacks $(LH)^q$ and $(HL)^q$ are added to the left and right sides of the structure $(LH)^2(2L2H)^{10}2L(HL)^2$, and the transmission peak positions of the resulting structure for number q from 0 to 12 are calculated (Fig. 6). The parameters used for the calculation are identical to that used for calculating the spectra shown in Fig. 5. The results show that the transmission peak positions of the structure $(LH)^q(LH)^2(2L2H)^{10}2L(HL)^2(HL)^q$ shift gradually to fixed ones when number q is increased from zero to a larger one. When number q is 4, the

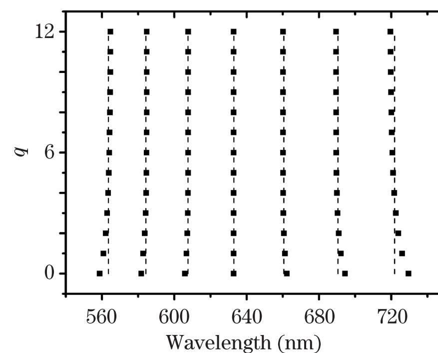

Fig. 6. Transmission peak positions of the structure $(LH)^q$ $(LH)^2(2L2H)^{10}2L(HL)^2(HL)^q$. The vertical dashed lines denote the reflection peak positions of the structure sub | $H(LH)^{13}(LH)^2(2L2H)^{10}2L(HL)^2Cr_{9.4}0.49H0.61L$.

transmission peaks are identical to the respective reflection peak positions of the structure sub | $H(LH)^{13}(LH)^2(2L2H)^{10}2L(HL)^2Cr_{9.4}0.49H0.61L$, not only at the central wavelength, but also at other wavelengths.

The shift of the transmission peak positions by means of increasing the number of LH and HL pairs can be attributed to the increase in the reflectivity of the flanking stacks, or the increase of the photonic potential barrier in a photonic quantum well (QW), as the finite photonic potential barrier plays different roles in confining the photonic levels in transmission mode of a photonic QW[11]. The deviation of the reflection peaks from the respective transmission peaks nearly diminishes when number q in the $(LH)^q$ and $(HL)^q$ stack is equal to 4 (Fig. 6). This implies that the barrier height of the structure sub | $H(LH)^{13}(LH)^2(2L2H)^{10}2L(HL)^2Cr_{9.4}0.49H$ $0.61L$ is equivalent to that of the structure $(LH)^4(LH)^2(2L2H)^{10}2L(HL)^2(HL)^4$. There is, however, a fundamental difference between the transmission and the reflection filters. The former is symmetric, the tunneling photons are traveling back and forth in the resonant chamber and are transmitted ultimately through the transmission filter. The latter is asymmetric, the tunneling photons are reflected entirely to the resonant chamber by the reflection mirror and transmitted ultimately through the induced-reflection match stack (IRMS) back to the incident medium.

The above-mentioned analysis can be inferred from more general cases where the middle structure is replaced by a QW constructed by flanking any dielectric film stack with reflection film stacks $(LH)^q$ and $(HL)^q$ of proper q. The position of the reflection peaks produced by the multi-wavelength high-reflection filters constructed by sandwiching such a middle structure between the reflection mirror and IRMS should be identical to that of the transmission peaks produced by the QW, provided that resonant transmission occurs at certain wavelengths in the well.

In conclusion, two types of multi-channel narrowband filters are proposed: transmittance-integrated narrowbandpass filter arrays, which are fabricated in one substrate by modifying the thickness of the spacer layer, and reflectance narrowband multi-channel filters, which utilize compound multilayer filters consisting of metal and dielectric materials. These types of filter show good filtering features and are potentially useful in many optical applications.

This work was supported by the National "863" Program of China.

References

1. Z. Wang, T. Sang, L. Wang, H. Jiao, Y. Wu, J. Zhu, L. Chen, S. Wang, X. Chen, and W. Lu, Appl. Opt. **47,** C1 (2008).
2. H. Jiao, Y. Wu, G. Tian, S. Wang, H. Cao, L. Zhang, and L. Fu, Appl. Opt. **46,** 867 (2007).
3. J. Stone and L. W. Stulz, Electron. Lett. **23,** 781 (1987).
4. G. E. Town, K. Sugden, J. A. R. Williams, I. Bennion, and S. B. Poole, IEEE Photon. Technol. Lett. **7,** 78 (1995).
5. R. Magnusson and S. S. Wang, Appl. Phys. Lett. **61,** 1002 (1992).
6. M. Kuznetsov, J. Lightwave Technol. **12,** 226 (1994).
7. D. Sadot and E. Boimovich, IEEE Commun. Mag. **36,** 50 (1998).
8. A. Piegari, J. Bulir, and A. K. Sytchkova, Appl. Opt. **47,** C151 (2008).
9. A. Piegari and J. Bulir, Appl. Opt. **45,** 3768 (2006).
10. Y. Wu, H. Jiao, D. Peng, Z. Wang, L. Fu, G. Lu, N. Chen, and L. Ling, Appl. Opt. **47,** 5370 (2008).
11. X. Chen, W. Lu, and S. C. Shen, Solid State Commun. **127,** 541 (2003).